Biochemistry

© Copyright 2000 by the American Chemical Society Volume 39, Number 44 November 7, 2000

Current Topics

Ion Channels, Permeation, and Electrostatics: Insight into the Function of KcsA

Benoît Roux,* Simon Bernèche, and Wonpil Im

Department of Biochemistry, Weill Medical College of Cornell University, 1300 York Avenue, New York, New York 10021

Received July 6, 2000; Revised Manuscript Received September 13, 2000

Highly specific membrane-spanning macromolecular structures, "ion channels", serve to facilitate and control the passage of selected ions across the lipid barrier (*1*). Without such specialized proteins, the hydrocarbon region of the lipid membrane would present a prohibitively high energy barrier to the passage of any ion (*2*). Recent progress in the determination of the structure of biological ion channels by X-ray crystallography gives a fresh impetus to efforts directed at understanding the fundamental principles governing ion permeation in molecular terms (*3*−*6*). Of particular interest was the determination of the structure of the KcsA K^+ channel from *Streptomyces lividan* (*5*). Because of its structural similarity to eukaryotic K channels (*7*), investigations of KcsA are expected to help improve the understanding of a large class of biologically important channels.

The complexity of ion channels is such that information extracted from computational models can contribute to the refinement of our understanding of ion channels. In recent years, molecular dynamics (MD) simulations with explicit solvent and membranes have been used to examine an increasing number of ion channels (*8*−*23*). Such computer simulations represent one of the most powerful approaches to studying ion permeation at the microscopic level. Nonetheless, models at any level are approximations. To make meaningful progress, it is important to choose computational approaches that incorporate the necessary amount of detail while avoiding superfluous complications. In this context, macroscopic continuum electrostatics models, in which the polar solvent is represented as a structureless dielectric medium, can be particularly useful since they reveal the dominant energetic factors related to ion permeation and, thus, can serve to illustrate fundamental principles in a particularly clear fashion.

Such an approach has a long history. In 1920, Born pioneered the application of continuum electrostatics for calculating the solvation free energy of spherical ions (*24*). The approach was later extended by Kirkwood (*25*) and Onsager (*26*) to treat arbitrary charge distributions inside a spherical cavity. With the use of powerful computers, the treatment of macromolecules of arbitrary shape was made possible by mapping the system onto a discrete grid and using finite-difference relaxation numerical algorithms to solve the Poisson−Boltzmann (PB) equation (*27*, *28*). As shown by comparisons to free energy simulations with explicit solvent, the approximation is remarkably successful in reproducing the electrostatic contribution to the solvation free energy of small solutes (*29*, *30*) or amino acids (*31*) (see ref *32* for a recent review of applications to biophysical systems).

In the following, we will briefly review the Born model and its microscopic basis. Fundamental electrostatics principles for ion permeation will then be described. Recent results on the KcsA K^+ channel obtained from the numerical solution to the PB equation will then be reviewed (*33*). Finally, some important limitations of continuum electrostatics will be discussed and illustrated.

MICROSCOPIC VIEW OF THE BORN MODEL

Born (*24*) calculated the solvation free energy of a spherical ion using a simple continuum electrostatic model

* To whom correspondence should be addressed. Telephone: (212) 746-6018. Fax: (212) 746-4843. E-mail: Benoit.Roux@med.cornell.edu.

10.1021/bi001567v CCC: $19.00 © 2000 American Chemical Society
Published on Web 10/13/2000

in which liquid water is represented as a structureless continuum dielectric medium. According to this model, the solvation free energy of an ion in water is

$$\Delta G_{\text{elec}} = \frac{1}{2}\frac{Q^2}{R_{\text{ion}}}\left(\frac{1}{\epsilon_{\text{w}}} - 1\right) \quad (1)$$

where Q is the charge of the ion, R_{ion} its radius, and ϵ_{w} the macroscopic dielectric constant of liquid water. The success of the Born model demonstrates that the solvation free energy of an ion in water is largely dominated by electrostatic interactions arising from the polarization of the high-dielectric solvent. However, to gain insight into the foundation of the model, it is necessary to examine how it arises from the microscopic level (*34*−*37*).

The electrostatic free energy of an ion, ΔG_{elec}, can be calculated as the reversible work for charging an ion in the solvent according to Kirkwood's thermodynamics integration (*38*)

$$\Delta G_{\text{elec}} = \int_0^Q \mathrm{d}Q' \left\langle \frac{\partial U}{\partial Q} \right\rangle_{(Q')} \quad (2)$$

Such an integral can be calculated by varying the ionic charge in MD free energy simulations (MD/FES) (*39*, *40*). Since the ion interacts with all the charges in the solvent molecules, the charging free energy can be written as

$$\Delta G_{\text{elec}} = \int_0^Q \mathrm{d}Q' \int \mathrm{d}\mathbf{r} \frac{1}{r} \langle \rho_{\text{elec}}(r;Q') \rangle \quad (3)$$

where the quantity $\langle \rho_{\text{elec}}(r;Q') \rangle$ is the average charge distribution function of the solvent around the ion with charge Q'. The solvent charge distribution function is sharply peaked at some distance r ($=R_{\text{ion}}$), which corresponds to the radius of the ion, and nearly zero everywhere else. Examples of the solvent charge distributions around K^+ and Cl^- calculated from MD simulations are shown in Figure 1. A reasonable approximation for deriving a closed form expression for ΔG_{elec} in eq 3 is to substitute the slowly varying integrand $1/r$ with its value at the dominant peak of the solvent charge distribution $1/R_{\text{ion}}$, yielding

$$\Delta G_{\text{elec}} \approx \int_0^Q \mathrm{d}Q' \frac{1}{R_{\text{ion}}} \int \mathrm{d}\mathbf{r} \langle \rho_{\text{elec}}(r;Q') \rangle \quad (4)$$

The remaining integral over the solvent charge distribution function can be evaluated in closed form. The total electrostatic potential at large distances is $Q'/\epsilon_{\text{w}}r$. By virtue of Gauss's theorem, this implies that the total charge enclosed by a spherical surface of radius r is Q'/ϵ_{w}. This corresponds to the charge of the ion, Q', and the charge arising from the solvent polarization, $Q'(1/\epsilon_{\text{w}} - 1)$. It follows that the total charge from the solvent obeys the sum rule

$$\int \mathrm{d}\mathbf{r} \langle \rho_{\text{elec}}(r;Q') \rangle = Q'\left(\frac{1}{\epsilon_{\text{w}}} - 1\right) \quad (5)$$

The Born model of ion solvation given in eq 1 is obtained after substitution of this expression in eq 4 followed by an integration over the charge Q', yielding $Q^2/2$.

At the atomic level, the solvent charge distribution function is distributed over a microscopic region of space of finite dimension (see Figure 1). This shows that the optimal value for the Born radius R_{ion} [which corresponds to the peak in $\langle \rho_{\text{elec}}(r;Q') \rangle$] is not a property of the ion alone. Ionic Born radii are effective parameters depending on both the charge of the ion and the atomic structure of the solvent molecules (*37*). They must be empirically adjusted to yield accurate solvation free energies.

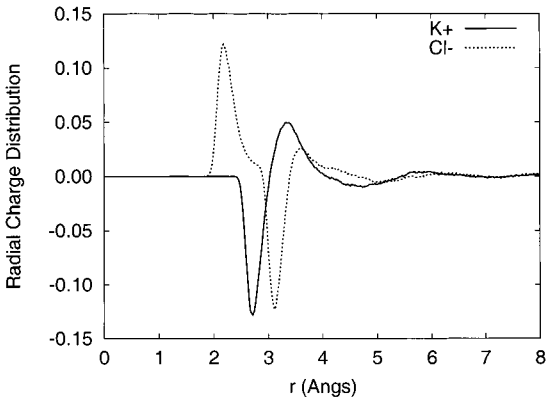

FIGURE 1: Radial distribution of the solvent charge around a K^+ and a Cl^- in bulk water. Around K^+ (—), the solvent charge distribution is dominated by the large negative peak at $r = 2.6$ Å arising from the electronegative oxygen of the surrounding water molecules. Around Cl^- (- - -), the solvent charge distribution is dominated by the large positive peak at $r = 2.2$ Å arising from the electropositive hydrogens of the surrounding water molecules; the peak at $r = 3.7$ Å arises from the second hydrogen in a water molecule. Details of the MD simulations were given in ref *78*.

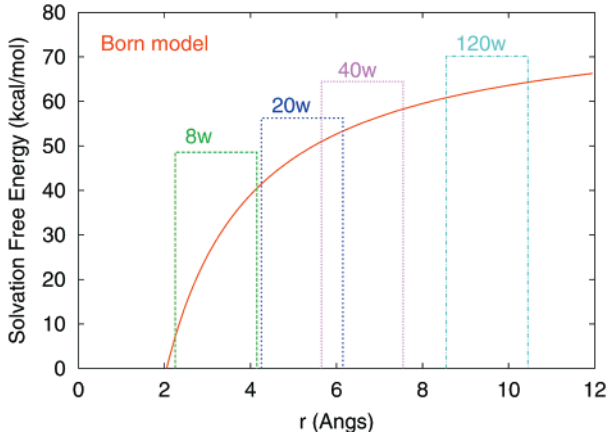

FIGURE 2: Solvation of K^+ in a small spherical droplet of water. The results from molecular dynamics free energy simulation (MD/FES) are compared with the Born model of solvation for a finite shell of high-dielectric material: $\Delta G = \Delta G_{\text{Born}} - Q^2(1/\epsilon_{\text{w}} - 1)/(2R_{\text{shell}})$. The MD/FES data were obtained with 10 simulation windows using the weighted histogram analysis method (WHAM) (*98*) from 400 ps trajectories generated with the program CHARMM (*51*). The parameters of the MD simulations and the Born radius have been adjusted such that both approaches yield a solvation free energy of −80 kcal/mol for an infinite bulk system.

One may question the ability of a continuum dielectric to represent the solvation by a small number of water molecules which is the typical condition of an ion in a molecular pore. This can be easily tested using MD/FES (*39*, *40*). The charging free energy of a K^+ ion in a small spherical droplet of 8, 20, 40, and 120 water molecules is shown in Figure 2. Remarkably, the results from MD/FES are qualitatively reproduced by the Born model. These calculations demonstrate that the continuum representation yields reasonable

results, even when the ion is solvated by a small number of water molecules.

ELECTROSTATICS AND ION PERMEATION

The Dielectric Barrier. Cell membranes are supramolecular sheetlike structures formed by lipid molecules possessing long nonpolar hydrocarbon chains attached to a polar moiety (*41*). The hydrocarbon chains of the lipid molecules form a 20−30 Å nonpolar (low-dielectric) core at the center of the bilayer. A pioneering study by Parsegian (*2*) helped reveal many of the essential electrostatics principles governing the passage of ions across the cell membrane. He calculated the free energy of transfer of an ion to the center of a planar membrane using a continuum electrostatic approximation. In his model, the nonpolar core formed by the hydrocarbon chains is approximated by a slab of featureless material having a dielectric constant of 2, while the aqueous solutions are represented by regions having a dielectric constant of 80. The main conclusion was that there is a large energy barrier (the "dielectric barrier") opposing the passage of an ion across the membrane.

To illustrate the important concept of the dielectric barrier, we calculated the free energy profile of a K^+ across a low-dielectric membrane. The electrostatic free energy of transfer of an ion of charge q_{ion} at a given position is calculated as

$$\Delta G_{elec} = \frac{1}{2} q_{ion} \phi \qquad (6)$$

where $\phi(i)$ is the electrostatic potential at the position of the ion for a particular configuration of the system. One may note that the factor of $^1/_2$ in eq 6, which is also present in eq 1 for the Born model, is characteristic of a linear dielectric response theory. The electrostatic potential is calculated by solving the Poisson−Boltzmann (PB) equation numerically using finite-difference methods (*27*, *28*)

$$\nabla[\epsilon(\mathbf{r})\nabla\phi(\mathbf{r})] - \bar{\kappa}^2(\mathbf{r})[\phi(\mathbf{r})] = -4\pi\rho_{syst}(\mathbf{r}) \qquad (7)$$

where $\epsilon(\mathbf{r})$ is the position-dependent dielectric constant, $\bar{\kappa}^2(\mathbf{r})$ is the position-dependent ionic screening constant, and $\rho_{syst}(\mathbf{r})$ is the charge density in the system. The result is shown in Figure 3 (salt effects were ignored in these calculations, and the screening constant was set to zero; further computational details are given in the figure caption).

It is observed that the presence of the high-dielectric aqueous region decreases the transfer energy only by a small amount; the free energy for transfer of an ion to the center of the membrane is about 38 kcal/mol, while the free energy for transfer to an infinite environment with a dielectric constant of 2 is on the order of 40 kcal/mol according to eq 1. The dielectric barrier is a fundamental impediment to ion permeation across cell membranes.

Ion channels are specialized proteins whose primary role is to help overcome the dielectric barrier presented by the cell membrane. As shown in Figure 3, even the presence of a featureless aqueous cylindrical pore 3 Å in diameter can help to reduce the dielectric barrier significantly (*42*). Although such a model cannot account for ionic selectivity, it highlights the importance of (high dielectric) water molecules along the permeation pathway. Since this early work, similar electrostatic calculations based on channel models with more complex shapes have been carried out (*43*, *44*). However, it is not possible to go much further without structural information about ion channels at the atomic level.

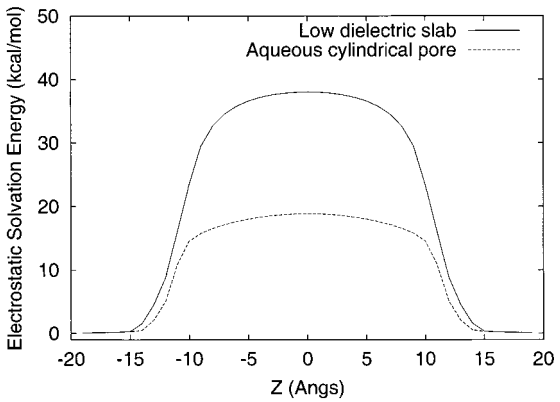

FIGURE 3: Illustration of the importance of the dielectric barrier. The solid line is the electrostatic reaction field free energy of a K^+ ion going across a 30 Å membrane represented by a structureless continuum medium with a dielectric constant of 2. The dashed line is the electrostatic reaction field free energy of a K^+ ion going through a 3 Å diameter cylindrical aqueous pore with a dielectric constant of 80. The finite-difference calculations were performed using the PBEQ module (*31*, *49*, *50*) of the biomolecular simulation program CHARMM (*51*). The numerical calculations were carried out using the standard relaxation algorithm (*27*, *28*). The complete system was mapped onto a cubic grid, and the Poisson equation was solved numerically. No electrolyte was included in the bulk solution. The total electrostatic potential was calculated at each point of the grid by solving the finite difference Poisson equation. The calculation was performed in two steps, first using a grid spacing of 1.0 Å (130^3 points, with periodic boundary conditions in the membrane plane), followed by a focusing around the main region with a grid spacing of 0.5 Å.

The Transmembrane Potential. The transmembrane potential acts as a driving force on the translocation of permeating ions and on the opening and closing transitions of voltage-gated channels. At the microscopic level, it arises from a small charge imbalance distributed in the neighborhood of the membrane−solution interface. In the simplest case of a perfectly planar membrane, the transmembrane electric field acting on the permeating ions is expected to be constant (*45*). A constant field is, however, probably inaccurate in the case of wide aqueous pores with irregular shapes. It is thus necessary to develop a more general treatment of the membrane potential.

To make progress, it is useful to separate the microscopic system into a pore region and two bulk regions. This formal separation is illustrated in Figure 4. For the sake of simplicity, we consider a situation with n ions at fixed positions $\mathbf{r}_i$ inside a molecular pore and a transmembrane voltage V_{mp}. The ionic solution on side I of the bulk region is in equilibrium with an electrode at zero potential, and the solution on side II of the bulk region is in equilibrium with an electrode at potential V_{mp}. All the ions in the pore region are represented explicitly, whereas it is assumed that they are represented implicitly in the bulk regions. On the basis of this construct, it can be shown that the total free energy has the form (*45*)

$$\Delta G_{tot} = \Delta G_0(\mathbf{r}_1, \mathbf{r}_2, ...) + \sum_i q_i \phi_{mp}(\mathbf{r}_i) + ... \qquad (8)$$

where ΔG_0 is the intrinsic free energy in the absence of any transmembrane potential and $\phi_{mp}(\mathbf{r})$ is the contribution from

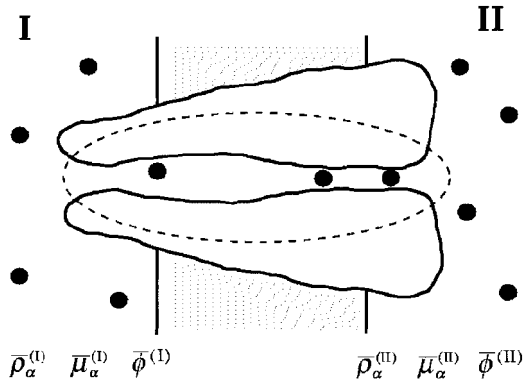

FIGURE 4: Schematic representation of an ion channel−membrane system with asymmetrical solutions on sides I and II. The "pore region", which corresponds to the ideally selective part of a channel, is highlighted with a dashed line. The "bulk region" corresponds to the remaining space in the system. The density of the permeable ions, the excess chemical potential, and the average electrostatic potential are $\bar{\rho}^{(S)}$, $\bar{\mu}^{(S)}$, and $\bar{\phi}^{(S)}$, respectively, on side S (I or II) of the membrane.

the potential difference across the membrane which is calculated from the modified PB equation (*45*)

$$\nabla[\epsilon(\mathbf{r})\nabla\phi_{mp}(\mathbf{r})] = 0 \text{ (pore region)}$$

$$\nabla[\epsilon(\mathbf{r})\nabla\phi_{mp}(\mathbf{r})] - \bar{\kappa}^2(\mathbf{r})[\phi_{mp}(\mathbf{r})] = 0 \text{ (bulk region, side I)} \quad (9)$$

$$\nabla[\epsilon(\mathbf{r})\nabla\phi_{mp}(\mathbf{r})] - \bar{\kappa}^2(\mathbf{r})[\phi_{mp}(\mathbf{r}) - V_{mp}] = 0 \text{ (bulk region, side II)}$$

where $\epsilon(\mathbf{r})$ and $\bar{\kappa}(\mathbf{r})$ are the space-dependent dielectric constant and Debye−Hückel screening factor, respectively, and V_{mp} is the equilibrium electrode potential far away on side II. The transmembrane potential ϕ_{mp}, acting on the ions in the pore region, arises from the long-range electrostatic interactions with the mobile ions in the bulk solutions on each side of the membrane outside the pore region (*45*). It may be noted that there is no screening factor $\bar{\kappa}(\mathbf{r})$ in the pore region because the ions are represented explicitly in this region. When $V_{mp} = 0$, the modified PB equation (eq 9) is reduced to the standard PB equation (eq 7), the transmembrane field is zero, and the total transfer free energy is equal to ΔG_0.

Interpretation of experimental ion-flux data is usually based on the assumption that the apparent voltage dependence arises from the rates of transition between discrete states of the system (*1*). The probability of such states is determined by the voltage-dependent free energy G_{tot} in eq 8. The fraction of the membrane potential affecting the probability of a given state is called the "electric distance". The spatial dependence of ϕ_{mp} cannot be observed experimentally. To transform the electric distance into a position, it is traditionally assumed that the transmembrane potential is linear along the channel axis and that the voltage dependence arises from the movement of a single ion (*1*). We will see below that this assumption is incorrect in the case of the KcsA channel.

KCSA CHANNEL

The general architecture of KcsA is shown in Figure 5. Briefly, the channel is made of four identical subunits of

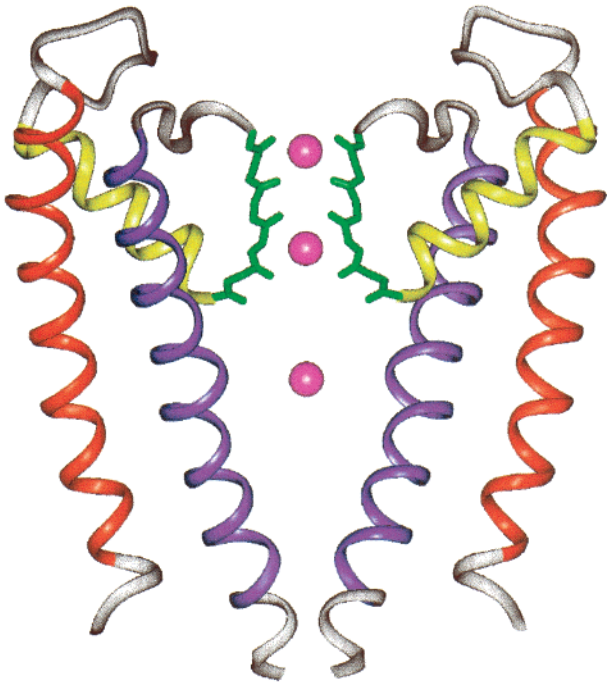

FIGURE 5: Schematic view of the KcsA channel based on the X-ray structure of Doyle et al. (*5*). The extracellular side is at the top, and the intracellular side is at the bottom. The main structural elements are the outer helix, the P-loop formed by the pore helix (residues 62−74) and the selectivity filter, and the inner helix. Three K^+ ions, located at the outer and inner sites of the selectivity filter and at the center of the central cavity, are shown. The membrane-bound channel is oriented to have the nonpolar residues in the lipid hydrocarbon core and the residues with aromatic side chains at the aqueous interface which is a recurrent feature of several membrane proteins (see refs *3*, *83*, *96*, and *97*). In this orientation, the outer K^+ binding site is at $Z = 17.2$ Å, the two inner sites are at $Z = 9.9$ Å (upper or outermost) and $Z = 6.6$ Å (lower or innermost), and the center of the water-filled cavity is precisely in the center of the hydrocarbon region of the bilayer ($Z = 0$ Å). The narrow hydrophobic region of the pore at the inner end of the teepee is located between $Z = -10.0$ and -20.0 Å.

three α-helices disposed symmetrically around a common axis corresponding to the pore. The narrowest part of the pore, formed by the backbone carbonyl oxygens of the TVGYG sequence, acts as a selectivity filter for K^+ ions. At the level of the bilayer center, the radius of the pore increases to form a 5 Å radius water-filled cavity lined by nonpolar residues. The size of the cavity is such that it could contain 20−40 water molecules (*5*, *19*−*23*). Four α-helices surrounding the pore (the "pore helices") are positioned approximately at an angle of 45° with respect to the pore axis so that they point directly toward the center of the cavity. Analysis of X-ray diffraction data in the presence of electron-dense rubidium shows that a cation occupies the center of the cavity, thus indicating that this is energetically favorable in the crystal structure. On the intracellular side of the channel end, the inner helices are joined together and the pore, lined by hydrophobic residues Thr107, Ala111, and Val115, narrows down to <3 Å in diameter.

The charging free energy of a K^+ in the center of the cavity was calculated using a continuum electrostatic approximation (*33*). The protein and the bound K^+ were represented explicitly with associated atomic charges and radii. The membrane was represented by a 24 Å slab corresponding to the width of the hydrocarbon core of the membrane (*46*).

Table 1: Calculated Free Energy (in kcal/mol) for the Transfer of a K^+ Ion from Bulk Water to the Cavity Center of KcsA[a]

charges included during transfer process	membrane	bulk water
no other charges	6.3	2.1
inner and outer ions	16.3	5.9
inner and outer ions and pore helices	−4.5	−1.4
inner and outer ions and all protein	−8.5	−3.4

[a] The pore helix consists of residues Tyr62−Thr74 in addition to the main chain atoms of Thr75, but excluding its carbonyl group. The side chain of Glu71 has been modeled in its protonated state. The atomic charges were taken from the all-hydrogen parameters PARAM22 program (*95*). The atomic radii used to define the protein−solvent dielectric boundary were derived from radial distribution functions calculated for the 20 standard amino acids from MD/FES with explicit water molecules (*31*). The Poisson−Botzmann equation was solved numerically with the finite-difference relaxation method (*27, 28*) implemented in the PBEQ module (*31, 49*) of the biomolecular simulation program CHARMM (*51*). The computational procedure is the same as that described in the legend of Figure 3.

The aqueous solution (including the water-filled cavity at the center of the channel) was represented in terms of a continuum media with a uniform dielectric constant of 80. A value of 2 was assumed for the dielectric constant of the protein interior; a value between 2 and 5 incorporates the influence of induced electronic polarization and small-amplitude librational atomic fluctuations (*47*, *48*).

The electrostatic contribution to the free energy of transfer of a K^+ to the center of the cavity is calculated as $\Delta G_{elec} = (G_{ic} - G_c - G_i)$, where G_{ic} is the electrostatic energy of the channel with a K^+ ion in the cavity, G_c is the electrostatic energy of the channel with no ion in the cavity, and G_i is the electrostatic energy of the K^+ ion in bulk water. The *G*'s are calculated as a sum over all the atomic charge of the protein and ions present in the system as in eq 6. The electrostatic potential for a given situation is computed by solving the PB equation numerically using finite-difference methods (*27, 28*). All the calculations were performed using the PBEQ module (*31*, *49*, *50*) which is implemented into the biomolecular simulation program CHARMM (*51*). In the following, we discuss the main results which are summarized in Table 1 (*33*).

Water-Filled High-Dielectric Cavity. To assess the influence of the irregular shape of the protein and the presence of the membrane interface, the free energy of transfer of one K^+ into the center of the cavity was calculated while all the charges in the system were turned off. The PB calculation yields the charging free energy contribution arising from the interaction of the ion with its own reaction field (the self-energy), a quantity corresponding conceptually to a Born charging energy, as given in eq 1, but taking into account the irregular molecular shape of the membrane channel system. The free energy of transfer calculated by solving the finite-difference PB equation is 6.3 kcal/mol. A simple estimate of the electrostatic solvation energy based on the Born model for the transfer of K^+ from aqueous solution to a 5 Å radius water-filled cavity surrounded by hydrocarbons is 16.2 kcal/mol. The result from the numerical calculation is smaller because the true shape of the cavity is not a sphere and because the ion interacts favorably with the bulk water regions. The transfer energy would be on the order of 20 kcal/mol if the cavity was not filled by water but instead by some material having a dielectric constant of 5 (*33*). These calculations emphasize the energetic stabilization brought about by the presence of the water-filled cavity.

Importance of Pore Helices. The water-filled high dielectric cavity localized at the center of the membrane helps reduce the electrostatic barrier for a permeating ion. Although the free energy is much lower than the very high value for transferring an ion from water to hydrocarbon (on the order of 60 kcal/mol; see above), it is nevertheless still very high. Furthermore, the transfer energy rises from from 6.3 to 16.3 kcal/mol when the two ions in the selectivity filter are included. Thus, the presence of an ion in the cavity would be energetically unfavorable without other interactions.

Most of the stabilization energy is provided by the four pore helices oriented toward the center of the cavity (see Figure 5). The transfer energy drops from 16.3 to −4.5 kcal/mol when the atomic charges of the pore helices are turned on (in the presence of the selectivity filter ions). The transfer energy decreases to −8.5 kcal/mol when the charge distribution of the entire protein is taken into account. Therefore, 80% of the total energy of stabilization by the protein results from the pore helices.

The magnitude of the contribution from the pore helices is striking and contrasts with generally accepted ideas about the influence of helix dipoles (*52*−*54*). Electrostatic effects due to helix dipoles are commonly thought to be very small and short-range. In the KcsA structure, the last carbonyl oxygen at C-terminus of the pore helices is 8 Å from the cation occupying the center of the cavity. Furthermore, the cavity is filled with high-dielectric water, which should shield the stabilizing electric field of the helix dipole. As a rough estimate, the energy for the interaction of a cation with one of the pore helices in liquid water would be on the order of only −0.14 kcal/mol; i.e., it is virtually insignificant.

The calculations show that the electrostatic stabilization due to the pore helices is magnified by the low-dielectric membrane environment. This is illustrated in Table 1 by setting the membrane dielectric constant to a value of 80 (as if the channel was a soluble protein). In this case, all the energies are attenuated. The low-dielectric membrane is thus the main reason the current results contrast with previous conclusions about the importance of the helix dipole reached on the basis of studies of water-soluble proteins. The calculations in Table 1 were performed using a value of 24 Å for the membrane thickness. Interestingly, the stabilization energy of a cation in the cavity depends on the thickness of the membrane. A detailed calculation shows that the stabilization decreases rapidly if the thickness of the membrane is less than 15 Å. The channel structure is optimal for a membrane with a thickness of 15−25 Å.

Electrostatic Stabilization of Monovalent Cations. So far, we have only considered the transfer of a monovalent cation representing K^+ to the cavity center. What about the stabilization of other ions? The electrostatic free energy of an ion in the cavity can be decomposed into reaction field and static field contributions. The general solution for the electrostatic free energy for transferring an ion of charge *Q* into an inhomogeneous medium with dielectric boundaries and static charges may be expressed as $\Delta\Delta G_{elec} = AQ^2/2 + BQ + C$, where *A* is the reaction field term, *B* is the static field term, and *C* is a constant term due to the influence of the dielectric constant of the ion on the protein charges (*C* is very small and can be neglected). The constant *A* depends

on the geometry and the size of the cavity. The constant B depends on the channel charge distribution, which is dominated by the pore helices. The reaction field is always destabilizing, whereas the static field is cation-attractive because of the pore helices. Our calculations allow us to evaluate the following constant values: $A = 12.5$, $B = -14.9$, and $C = 0.1$.

In the case of a divalent cation ($Q = 2$), the transfer free energy is −4.6 kcal/mol, significantly less favorable than for a monovalent cation. The optimal charge for which the transfer is most favorable is obtained by differentiating the free energy with respect to the ion charge, yielding $-B/A = 1.2$ unit charge. Thus, the KcsA K^+ channel is tuned to preferably stabilize a monovalent cation at the center of the membrane. The specificity for monovalent cations results from the size and shape of the high-dielectric cavity (constant A) as well as the magnitude of the field provided by the pore helices (constant B).

The biological function of such tuning is clear. The K^+ selectivity filter is located at the extracellular end of the pore (*5*). Cations other than K^+ could enter from the cytoplasm, penetrate two-thirds of the way across the membrane, and block the pore at the selectivity filter. The valence selectivity of the cavity favors monovalent cations over intracellular polyvalent cations. The abundance of K^+ compared to Na^+ inside the cell ensures that the monovalent cation in the cavity is predominantly K^+. Inward rectifying K^+ channels are susceptible to blocking by cytoplasmic polyvalent cations such as Mg^{2+} (*55*, *56*) and polyamines (*57*). Consequently, when the electrochemical driving force for K^+ favors flow outward across the cell membrane, the pore of these channels becomes occluded. This property is central to the operation of inward-rectifier K^+ channels. It turns out that these K^+ channels have a polar residue (Asn or Asp) at the position of an amino acid that lines the wall of the cavity (*55*, *56*). In other words, the inward-rectifier K^+ channels have a modified static field (constant B) to permit blocks by multivalent cations.

To further illustrate the mechanism of inward rectification, we calculated the free energy for transfer of monovalent and divalent cations to the central cavity of KcsA in which this residue was substituted with an Asn or an Asp. Alignment of the amino acid sequence of inward rectifiers with respect to that of KcsA is not straightforward due to the very low degree of similarity, though it suggests that the polar residue Asn or Asp is located along the inner helix, facing the cavity (*58*). In KcsA, this position may reasonably correspond to Gly104 (though alternatives are possible). Results from preliminary calculations show that the cavity is increasingly favorable for a divalent cation to a monovalent cation when a polar residue is present, though the actual transfer free energy is very large with four unprotonated Asp residues (i.e., on the order of −100 kcal/mol). Despite the significant uncertainty about the assumed structural similarity between KcsA and inward rectifiers (*59*), this unphysically large energy might indicate that not all the Asp side chains from the four monomers can be ionized simultaneously in the cavity.

Ion−Ion Repulsion. Ion−ion repulsion plays an important role in the conduction mechanism of K channels (*60*, *61*). The high affinity of the ions for the channel, which is responsible for the selectivity, is balanced by ion−ion repulsion to achieve a high throughput. The determination of the structure of the KcsA K^+ channel with X-ray showed that the pore contains multiple permeant ions (*5*). In particular, the ion at the center of the cavity is less than 7 Å away from the ion in the (innermost) inner binding site. How is its free energy affected by the presence of the other ions in the pore? In liquid water, the energy for the interaction between two K^+ ions at this distance would be $q^2/\epsilon_w r$ (=0.59 kcal/mol), i.e., on the order of $k_B T$, the thermal energy. Such a simple Coulombic law is inappropriate in the present case. In a complex environment with irregular dielectric boundaries, the magnitude of ion−ion repulsion is determined by the interaction of the ions with the reaction fields. Continuum electrostatic calculations based on the PB equation can be used to answer such a question.

In the presence of two K^+ ions in the selectivity filter, the free energy of transfer to the center of the cavity is −8.5 kcal/mol. In their absence, the free energy decreases to −19.0 kcal/mol; hence, the repulsion is on the order of 10 kcal/mol. It may be noted that the effective repulsion is the same with all protein charges turned off; the energy of transfer from ion increases from 6.3 to 16.3 kcal/mol (see Table 1) because the same three-dimensional conformation is used for all the states of occupancy in the electrostatic calculations. Although the repulsion between a K^+ ion in the cavity and the two K^+ ions in the selectivity filter is significant, the net transfer free energy of an ion in the cavity in the presence of two ions in the selectivity filter remains highly favorable due to the influence of the pore helices. In fact, a free energy of −8.5 kcal/mol may seem somewhat inconsistent with the high throughput of K^+ channels (*1*). In a multi-ion pore, the large favorable ion−channel interaction is expected to be compensated by ion−ion repulsion. Recent results from MD simulations of the KcsA channel provide some clues. During the trajectory, a concerted transition leading to a state with no ion in the cavity and three K^+ ions in the selectivity filter occurred spontaneously (*23*). What would be the probability of having a fourth ion entering from the intracellular side into the cavity in this configuration? The calculated free energy for transfer of a fourth K^+ ion from the bulk solution to the center of the cavity with three K^+ ions in the selectivity filter is on the order of 0.0 kcal/mol. This implies that the entry of a fourth ion into a pore occupied by three ions is not hindered by a large free energy. Therefore, the calculations suggest that the repulsion from a fourth ion might be necessary to compensate for the high affinity for the channel and to achieve a high throughput.

Ion Entry from the Inner Side. The KcsA channel is mostly closed at neutral pH, but it can be stabilized in the open state at low intracellular pH (*62*−*64*). Data from electron paramagnetic spectroscopy (EPR) suggests that the opening and closing of the channel involve the movements of the inner helices which presumably would result in a change in the diameter of the narrow pore lined by hydrophobic residues (*63*). MD simulations of KcsA in a lipid bilayer indicate that the packing of the inner helices is very stable (*23*).

The passage of a dehydrated cation through this narrow hydrophobic channel is sterically possible. However, it would require a nearly complete dehydration and should be energetically prohibited (though such event has been observed once during a MD trajectory; see ref *65*). To illustrate

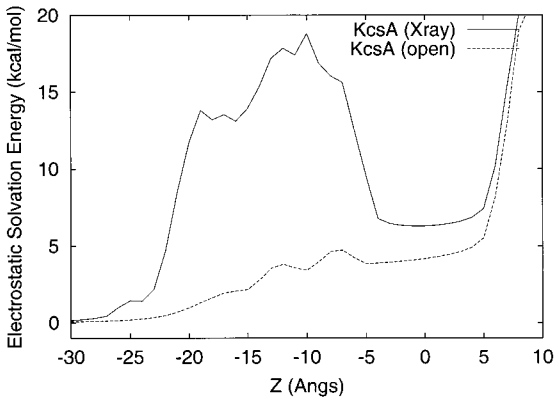

FIGURE 6: Electrostatic energy profile through the inner mouth of KcsA. All charges other than that of K1 have been turned off for the sake of illustrating the dominant reaction field contribution. The result for the X-ray structure (—) and an atomic model of the open state are shown. The diameter of the pore on the inner side of the open state model is increased by 3 Å relative to that in the X-ray structure. The computational procedure is described in the legend of Figure 3.

the influence of the diameter of the intracellular entrance, the energy profile along the axis of the crystallographic structure of KcsA and a model of the open state was determined using continuum electrostatics. Although there is no detailed three-dimensional atomic resolution structure of the KcsA channel in the open state, it is possible to construct a crude model in accord with the current observations. The model was refined using MD and energy minimization in the presence of artificial harmonic energy restraints designed to increase the diameter of the pore on the inner side by only 3 Å relative to the X-ray structure. The results are shown in Figure 6 (all other charges have been turned off or the sake of illustrating the dominant reaction field contribution).

It is observed that an ion going through the narrow inner entrance of the X-ray structure is experiencing an energy barrier of almost 20 kcal/mol due to the electrostatic reaction field. This demonstrates that the pore in the crystallographic structure of KcsA is effectively closed at the intracellular end of the channel. Remarkably, increasing the diameter of the inner entrance by only 3 Å is enough to reduce the large energy barrier from 20 to ~3−4 kcal/mol. Therefore, even very small movements of the inner helices can affect the free energy landscape for ion entrance significantly, effectively closing or opening the channel.

Ionization State of Glu71. The side chain of Glu71, a residue which is near the selectivity filter, could not be detected in the electron density, and its atomic coordinates were not determined (*5*). It has been suggested that it is in a protonated (neutral) state, forming a diacid hydrogen bond with the carboxylate group of Asp80 (*23*). Clearly, the presence of four negatively charged side chains near the selectivity filter can alter significantly the stability of cations in the channel. For example, the free energy of the K^+ ion in the outer site is further stabilized by −6 kcal/mol when the Glu71 side chains of the four monomers are unprotonated. Determining the correct ionization state of Glu71 is thus essential for meaningful MD simulations of the ion conduction mechanism (*19*−*23*).

Continuum electrostatic calculations can be used to estimate the relative stability of the protonated and unprotonated states of ionizable side chains in the complex dielectric environment (*66*, *67*). The method for estimating the pK_a of the residue is based on calculating, for both the protonated (p) and unprotonated (u) state of a residue, the difference between its electrostatic free energy when it is in the protein environment and its electrostatic free energy when it is isolated in solution. The pK_a shift (relative to the intrinsic pK_a of the same amino acid isolated in solution) is given by

$$\Delta \mathrm{p}K_a = -\frac{\Delta\Delta G}{2.3 k_B T} \quad (10)$$

where

$$\Delta\Delta G = [\Delta G_{\mathrm{protein}}(\mathrm{p}) - \Delta G_{\mathrm{protein}}(\mathrm{u}) - \Delta G_{\mathrm{isolated}}(\mathrm{p}) + \Delta G_{\mathrm{isolated}}(\mathrm{u})] \quad (11)$$

In particular, such methods have been applied to ionizable residues of bacterial porins (*68*), models of the pore-forming region of the nicotinic acetylcholine receptor (*69*), and the influence of pH on the cation versus anion selectivity of alamethicin channels (*70*).

The ionization state of Glu71 in KcsA was examined using the PB equation (all computational details are the same as described above). According to the calculations, the protonated state of Glu71 in KcsA is stabilized by −14.6 kcal/mol relative to the unprotonated state. This implies a pK_a shift of nearly 10.5, indicating that the glutamic acid side chain should be protonated under normal conditions at pH 7. This value was obtained by assuming that the three other Glu71 residues are protonated and that ions are present in the channel. A pK_a shift of 14.9 is obtained when the Glu71 side chains of the three other monomers are in an ionized state. The pK_a of Glu71 is slightly perturbed by the presence of ions in the channel; the pK_a shift increases to 16.1 if no ions are present in the channel (assuming that the three other Glu71 residues are neutral). In all cases, the results presented here suggest that the side chain of Glu71 should be protonated. Combined efforts from experimental and computational studies will be required to resolve detailed questions concerning the ionization state(s) of the channel.

Transmembrane Potential. The transmembrane potential profile along the axis of the KcsA channel was calculated using the modified PB theory based on eq 9. To further examine the influence of a conformational change in the channel, the transmembrane potential profile was calculated for the X-ray structure and for the structural model of the open state that was described above. The results are shown in Figure 7. The values of the potential at functionally important sites along the channel axis are summarized in Table 2.

The calculated profile of the transmembrane electric potential can be compared with experimental estimates based on single-channel recordings by Neyton and Miller (*61*, *66*). They analyzed the membrane voltage dependence of the effects exerted by K^+ on Ba^{2+} blockade to obtain an estimate of the distance that an ion must travel through the transmembrane electric potential to reach a specific binding site. It was concluded that there is a first binding site external to Ba^{2+} near the extracellular solution (the external lock-in site) which is highly selective for K^+ and that there is a second binding site, again external to Ba^{2+} but deeper in the pore

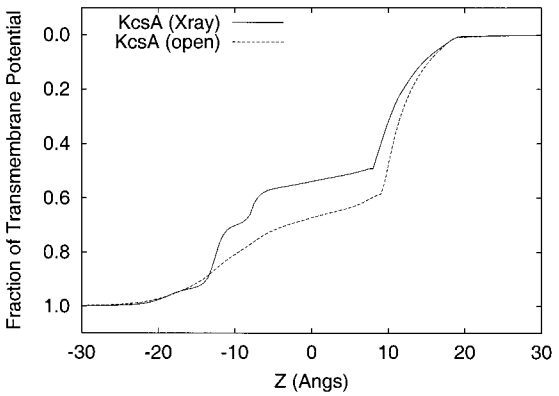

FIGURE 7: Fraction of the transmembrane potential (relative to the extracellular solution) along the axis of KcsA. The modified PB equation (eq 9) was implemented in the PBEQ module (*31*, *50*, *49*) of the biomolecular simulation program CHARMM (*51*) and was solved numerically using the procedure described in ref (*45*) and in the legend of Figure 3.

Table 2: Calculated Fraction of the Transmembrane Potential along the Channel Axis[a]

position along the channel axis	X-ray structure (closed state)	model of open state
outer site	0.04	0.05
upper inner site	0.32	0.49
lower inner site	0.50	0.62
cavity	0.54	0.68

[a] All conditions are the same as those described in Table 1 with an additional ionic screening from 150 mM salt; the positions of the sites along the channel axis are taken from the legend of Figure 5.

(the enhancement site) which is also highly selective for K^+. The external lock-in and enhancement sites were highly selective for K^+ and appeared to reside 15 and 50%, respectively, of the way across the membrane electric potential difference relative to the external solution, while an internal lock-in site exhibited little ion selectivity and appeared to reside approximately 70% of the way across the membrane. Recently, Jiang and MacKinnon showed that Ba^{2+} binds at the innermost of the inner sites of KcsA using X-ray crystallography (*71*). On the basis of this result, they argued that the outer binding site and the large cavity correspond to the external and internal lock-in sites of Neyton and Miller, respectively.

The agreement of the calculated membrane potential given in Table 2 with the estimates from Neyton and Miller (*60*, *61*) is remarkable. This is particularly true for the calculations based on the open state model. According to the current calculations, the calculated fraction of the potential at the outer site (external lock-in site) is 0.05 relative to the external solution. The fraction of the potential in the upper inner site (enhancement site) is 0.32 for the X-ray structure and 0.49 for the open state model. The fraction of the potential in the cavity center (internal lock-in site) is 0.54 for the X-ray structure and 0.68 for the open state model. The fraction of the potential at the lower inner site, where the Ba^{2+} binds, is 0.50 for the X-ray structure (closed state) and 0.62 for the open state model. It may be noted that this interpretation of the data is based on the assumption that the apparent voltage dependence arises from a single ion while the ions in the pore presumably move in a somewhat concerted fashion (*19*−*23*). Nevertheless, it is encouraging to find such consistency with the experimental estimates.

Interestingly, the calculations show that a conformational change with no displacement of the ions can be coupled to the transmembrane potential. According to our calculation, a transition from the open to the closed state occurring while the channel is occupied by three ions (cavity and inner and outer sites) would correspond electrically to the movement of one ion over 30% of the potential difference across the membrane. Yet, no ions are displaced. The variation arises solely from a modification of the dielectric boundaries in the system. Furthermore, this implies that the open state is stabilized by a transmembrane potential. It may be possible that the opening and closing transitions of voltage-gated channels reflect similar effects with permeant ions captured in the interior of the closed channel (*72*).

LIMITATIONS OF A CONTINUUM REPRESENTATION

In the previous sections, we have described the microscopic basis of the Born model and discussed applications of continuum electrostatics to ion permeation and the KcsA K^+ channel. Clearly, the Born model can capture the dominant features of the energetics of ion solvation even in the case of finite droplets of water molecules (see Figure 2). However, ion selectivity is exquisitely sensitive to small energetic factors (*1*). Therefore, one has to be careful in applying continuum electrostatics to ion permeation since this may very well take the approximation beyond its range of validity. For example, MD simulations indicate that the configurational freedom of water molecules is reduced in the confined environment of a narrow pore (*18*, *73*−*75*). This has been shown to strongly affect the dielectric response in aqueous pores (*76*, *77*) as well as ion−channel and ion−ion interactions (*78*−*81*).

The well-characterized gramicidin A (GA) channel offers a unique model system for trying to address questions concerning the energetics of ion permeation at the molecular level and examine the limitations of a continuum representation (for a review of the GA channel, see ref *82*). In the following, we will try to illustrate some of the limitations of continuum electrostatics and review briefly the results of two MD/FES studies based on atomic models of the GA channel (*78*, *79*).

Cation versus Anion Specificity of the GA Channel. One of the simplest forms of ion selectivity is the valence specificity of the GA channel. The GA channel is ideally selective for cations, while it is virtually impermeable to anions (*1*, *82*). Since all the side chains of the GA channel are nonpolar, no obvious mechanism for charge discrimination is suggested on the basis of its three-dimensional structure (*83*).

The free energy difference of K^+ and Cl^- for the interior of the channel was calculated using MD/FES based on atomic models of bulk water and of a GA-like channel (*78*) (K^+ and Cl^- were chosen for the sake of simplicity because their solvation free energies are both on the order of −80 kcal/mol in liquid water; see ref *80*). The result of the calculation shows that the environment of the pore interior is particularly unfavorable for anions relative to cations. The relative free energy, $G_{Cl}(GA) - G_{Cl}(water) - G_K(GA) + G_K(water)$,

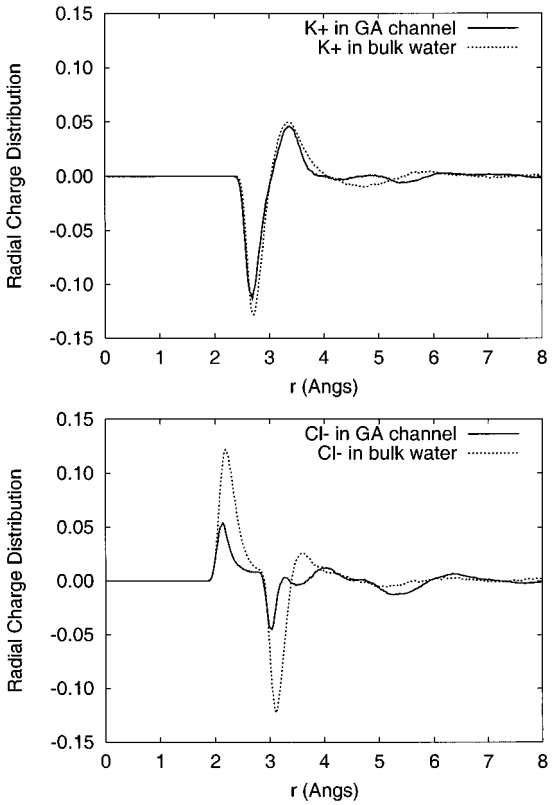

FIGURE 8: Radial distribution of the solvent charge around a K^+ (top) and a Cl^- (bottom) in bulk water (—) and in a GA-like channel (- - -). The details of the MD simulations are given in ref *78*.

obtained from MD/FES calculations is on the order of almost +60 kcal/mol (*78*). Thus, Cl^- has a much lower affinity for the interior of the channel than K^+, even though they the same solvation free energy in bulk water.

The large free energy difference can be understood by considering the average charge radial distribution around the ions. The charge distribution function of K^+ and Cl^- in bulk water and in the GA channel is shown in Figure 8 (the results for the ion solvation in bulk water were also shown in Figure 1). In bulk water, the K^+ ion is surrounded by approximately 7.4 water molecules in the first solvation shell; the oxygen of the water molecules points toward the ion, causing a negative peak at a contact distance of 2.6 Å which provides a favorable electrostatic interaction energy. In the channel, the solvation is provided primarily by the oxygen of the backbone carbonyl group. Although the two environments are significantly different, the resulting charge distributions around K^+ are remarkably similar. In contrast, the radial charge distribution is markedly different in bulk water and in the channel in the case of a Cl^- ion. In bulk solution, the water molecules provide a favorable electrostatic interaction energy by forming hydrogen bonds with the anion. In the channel, similar hydrogen bonds with the NH amide backbone group are not easily formed. Thus, although the channel is electrically neutral, the strong asymmetry in the permanent charge distribution of the peptide backbone results in a significant reduction of favorable interaction energy in the channel for negatively charged ions.

Ion—Ion Interactions and a Doubly Occupied GA Channel. Several lines of evidence indicate that the GA channel can be occupied simultaneously by two ions, one ion in each binding site near the channel's end (see ref *79* for a review).

Table 3: Relative Free Energy of Double Occupancy in the GA Channel (kcal/mol)[a]

ion	$\Delta\Delta G$	contribution from single-file water	contribution from GA carbonyl oxygens
Li^+	0.0	0.0	0.0
Na^+	−2.4	−1.9	0.1
K^+	−3.8	−4.9	1.4
Rb^+	−3.3	−5.6	2.5
Cs^+	−3.6	−5.9	3.2

[a] All free energies are given relative to Li^+. Details of the MD/FES simulations were given in ref *79*.

Interpretation of these experimental observations has led to the view that although double occupancy of the GA channel is less favorable than single occupancy for all cations, it is relatively more favorable for the large cations (K^+, Rb^+, and Cs^+) than for the small ones (Li^+ and Na^+). Simple considerations based on continuum electrostatics cannot account for the observed trend because the two cation binding sites are separated by almost 20 Å (*84—87*).

The relative single-to-double occupancy free energy was calculated using MD/FES for the five cations Li^+, Na^+, K^+, Rb^+, and Cs^+ (*79*). The results are given in Table 3. The calculations revealed, in agreement with experimental observations, that the doubly occupied state is relatively more favorable for the larger ions. According to MD/FES, the repulsion energy between two Na^+ ions occupying the binding sites in the GA channel is nearly 1.5 kcal/mol larger than the corresponding repulsion between two K^+ ions. This is remarkable given the fact that the cations in a doubly occupied GA channel are separated by a distance on the order of 20 Å. In liquid water, the ion—ion interaction would be well-approximated by a shielded Coulombic law $q^2/\epsilon_w r$ (independent of the ionic radius), at such a distance. However, the situation is very different in the case of the narrow GA channel. Analysis of the simulations indicates that the difference in free energy arises from the properties of the six water molecules disposed in single file inside the narrow channel. Small cations such as Li^+ and Na^+ are relatively better solvated in the singly occupied state than in the doubly occupied state, while bigger cations such as K^+, Rb^+, and Cs^+ are solvated almost as well in both the singly and doubly occupied states. The calculations show that ion—ion interactions are affected, in a nontrivial way, by the environment of a narrow molecular pore.

SUMMARY

There is no doubt that MD simulations in which water and lipid molecules are treated explicitly represent the most detailed method for studying ion channels. Nevertheless, this computationally intensive methodology often suffers from statistical uncertainties due to finite sampling. From this perspective, a continuum model can be very useful for examining various energetic factors arising from long-range electrostatic effects involved in the function of an ion channel. This review shows that relatively simple numerical calculations based on continuum electrostatic models can be used to characterize ion—channel interactions, ion—ion repulsion, and the transmembrane potential profile, thus, providing very valuable insight into the function of the KcsA channel.

Nonetheless, it is also important to recognize the limitations of the continuum approximation and use it only within its range of validity. Those were illustrated with MD/FES calculations applied to the GA channel. The results indicate that a continuum approximation cannot realistically account for ion−channel and ion−ion interaction in the confined environment of a narrow selectivity filter. Atomic models are and will remain necessary for addressing such detailed questions.

Our focus in the current review has been exclusively on equilibrium energetics. Ion fluxes are, of course, observed under nonequilibrium conditions. In the future, it will be important to take thoses aspects of the problem into consideration. It is likely that a combination of approaches, including continuum electrostatics based on the PB equation, MD and MD/FES calculations (see refs *8*−*23*, *87*, *88*), and Brownian dynamics simulations (*89*−*92*), as well as continuum theories of electrodiffusion (*93*, *94*) will contribute to refining our understanding of ion permeation in the future.

REFERENCES

1. Hille, B. (1992) *Ionic Channels of Excitable Membranes*, 2nd ed., Sinauer, Sunderland, MA.
2. Parsegian, A. (1969) Energy of an ion crossing a low dielectric membrane: Solution to four relevant electrostatic problems, *Nature 221*, 844−846.
3. Cowan, S. W., Schirmer, T., Rummel, G., Steiert, M., Gosh, R., Pauptit, R. A., Jansonius, J. N., and Rosenbusch, J. P. (1992) Crystal structures explain functional properties of two *E. coli* porins, *Nature 358*, 727−733.
4. Chang, G., Spencer, R. H., Lee, A. T., Barclay, M. T., and Rees, D. C. (1998) Structure of the mscl homolog from *Mycobacterium tuberculosis*: a gated mechanosensitive ion channel, *Science 282*, 2220−2226.
5. Doyle, D. A., Cabral, J. M., Pfuetzner, R. A., Kuo, A., Gulbis, J. M., Cohen, S. L., Chait, B. T., and MacKinnon, R. (1998) The structure of the potassium channel: molecular basis of K^+ conduction and selectivity, *Science 280*, 69−77.
6. Toyoshima, C., Nakasako, M., Nomura, H., and Ogawa, H. (2000) Crystal structure of the calcium pump of sarcoplasmic reticulum at 2.6 Å resolution, *Nature 405*, 647−655.
7. MacKinnon, R., Cohen, S. L., Kuo, A., Lee, A., and Chait, B. T. (1998) Structural conservation in prokaryotic and eukaryotic potassium channels, *Science 280*, 106−109.
8. Roux, B., and Karplus, M. (1994) Molecular Dynamics Simulations of the Gramicidin Channel, *Annu. Rev. Biomol. Struct. Dyn. 23*, 731−761.
9. Woolf, T. B., and Roux, B. (1994) Molecular dynamics simulation of the gramicidin channel in a phospholipid bilayer, *Proc. Natl. Acad. Sci. U.S.A. 91*, 11631−11635.
10. Chiu, S. W., Subramaniam, S., and Jakobsson, E. (1999) Simulation study of a gramicidin/lipid bilayer system in excess water and lipid. I. Structure of the molecular complex, *Biophys. J. 76*, 1929−1938.
11. Zhong, Q., Moore, P. B., Newns, D. M., and Klein, M. L. (1998) Molecular dynamics study of the LS3 voltage-gated ion channel, *FEBS Lett. 427*, 267−270.
12. Zhong, Q. F., Jiang, Q., Morre, P. B., Newns, D. M., and Klein, M. L. (1998) Molecular dynamics simulation of a synthetic ion channel, *Biophys. J. 74*, 3−10.
13. Tieleman, D. P., Berendsen, H. J. C., and Sansom, M. S. P. (1999) An alamethicin channel in a lipid bilayer: molecular dynamics simulations, *Biophys. J. 76*, 1757−1769.
14. Sansom, M. S. P., Kerr, I. D., Smith, G. R., and Son, H. S. (1997) The influenza A virus M2 channel: A molecular modeling and simulation study, *Virology 233*, 163−173.
15. Zhong, Q. F., Husslein, T., Moore, P. B., Newns, D. M., Pattnaik, P., and Klein, M. L. (1998) The M2 channel of influenza A virus: A molecular dynamics study, *FEBS Lett. 434*, 265−271.
16. Suenaga, A., Yamato, I., and Saito, M. (1997) Molecular dynamics simulation of outer membrane porins in *Escherichia coli*, in *Towards Molecular Biophysics of Ion Channels* (Sokabe, M., Auerbach, A., and Sigworth, F., Eds.) pp 217−232, Elsevier, Amsterdam.
17. Suenaga, A., Komeiji, Y., Uebayasi, M., Meguro, T., Saito, M., and Yamato, I. (1998) Computational observation of an ion permeation through a channel protein, *Biosci. Rep. 18*, 39−48.
18. Tieleman, D. P., and Berendsen, H. J. C. (1998) A Molecular Dynamics Study of the Pores Formed by *E. coli* OmpF Porin in a Fully Hydrated POPE Bilayer, *Biophys. J. 74*, 2786−2801.
19. Guidoni, L., Torre, V., and Carloni, P. (1999) Potassium and sodium binding to the outer mouth of the K^+ channel, *Biochemistry 38*, 8599−8604.
20. Allen, T. W., Kuyucak, S., and Chung, S. H. (1999) Molecular dynamics study of the KcsA potassium channel, *Biophys. J. 77*, 2502−2516.
21. Shrivastava, I. H., and Sansom, M. S. (2000) Simulations of ion permeation through a potassium channel: molecular dynamics of KcsA in a phospholipid bilayer, *Biophys. J. 78*, 557−570.
22. Aqvist, J., and Luzhkov, V. (2000) Ion permeation mechanism of the potassium channel, *Nature 404*, 881−884.
23. Berneche, S., and Roux, B. (2000) Molecular dynamics of the KcsA K(+) channel in a bilayer membrane, *Biophys. J. 78*, 2900−2917.
24. Born, M. (1920) Volumen und hydratationswarme der ionen, *Z. Phys. 1*, 45−48.
25. Kirkwood, J. G. (1934) Theory of solution of molecules containing widely separated charges with application to zwiterions, *J. Chem. Phys. 2*, 351.
26. Onsager, L. (1936) Electric Moment of Molecules in Liquids, *J. Am. Chem. Soc. 58*, 1468−1493.
27. Warwicker, J., and Watson, H. C. (1982) Calculation of the electric potential in the active site cleft due to α-helix dipoles, *J. Mol. Biol. 157*, 671−679.
28. Klapper, I., Hagstrom, R., Fine, R., Sharp, K., and Honig, B. (1986) Focusing of electric fields in the active site of Cu-Zn superoxide dismutase: effects of ionic strength and amino-acid modification, *Proteins 1*, 47.
29. Jean-Charles, A., Nicholls, A., Sharp, K., Honig, B., Tempczyk, A., Hendrickson, T., and Still, W. C. (1991) *J. Am. Chem. Soc. 113*, 1454−1455.
30. Sitkoff, D., Sharp, K. A., and Honig, B. (1994) Accurate calculation of hydration free energies using macroscopic solvent models, *J. Phys. Chem. 98*, 1978.
31. Nina, M., Beglov, D., and Roux, B. (1997) Atomic Radii for Continuum Electrostatics Calculations based on Molecular Dynamics Free Energy Simulations, *J. Phys. Chem. B 101*, 5239−5248.
32. Honig, B., and Nicholls, A. (1995) Classical electrostatics in biology and chemistry, *Science 268*, 1144.
33. Roux, B., and MacKinnon, R. (1999) The cavity and pore helices in the KcsA K^+ channel: electrostatic stabilization of monovalent cations, *Science 285*, 100−102.
34. Rashin, A. A., and Honig, B. (1985) Reevaluation of the Born model of ion hydration, *J. Phys. Chem. 89*, 5588.
35. Hirata, F., Redfern, P., and Levy, R. M. (1988) Viewing the born model for ion hydration through a microscope, *Int. J. Quant. Chem: Quant. Biol. Symp. 15*, 179.
36. Jayaram, B., Fine, R., Sharp, K., and Honig, B. (1989) Free energy calculations of ion hydration: an analysis of the born model in terms of microscopic simulations, *J. Phys. Chem. 93*, 4320.
37. Roux, B., Yu, H. A., and Karplus, M. (1990) Molecular Basis for the Born Model of Ion Solvation, *J. Phys. Chem. 94*, 4683−4688.
38. Kirkwood, J. G. (1935) Statistical mechanics of fluid mixtures, *J. Chem. Phys. 3*, 300−313.
39. Kollman, P. A. (1993) Free Energy Calculations: Applications to Chemical and Biochemical Phenomena, *Chem. Rev. 93*, 2395−2417.

40. McCammon, J. A., and Straatsma, T. P. (1992) Alchemical free energy simulation, *Annu. Rev. Phys. Chem. 43*, 407.
41. Gennis, R. B. (1989) *Biomembranes: molecular structure and functions*, Springer-Verlag, New York.
42. Jordan, P. C. (1981) Energy barriers for passage of ions through channels. Exact solution of two electrostatic problems, *Biophys. Chem. 13*, 203−212.
43. Jordan, P. C. (1984) The total electrostatic potential in a gramicidin channel, *J. Membr. Biol. 78*, 91−102.
44. Jordan, P. C., and Vayl, I. S. (1985) How shortening a channel may lower its conductance. The case of des-Val^7-*d*Val^8-gramicidin A, *Biochim. Biophys. Acta 818*, 416−420.
45. Roux, B. (1999) Statistical mechanical equilibrium theory of selective ion channels, *Biophys. J. 77*, 139−153.
46. White, S. H., and Wiener, M. C. (1996) The liquid crystallographic structure of fluid lipid bilayer membranes, in *Biological Membranes. A molecular perspective from computation and experiment* (Merz, K. M., and Roux, B., Eds.) pp 127−144, Birkhauser, Boston.
47. Gilson, M. K., and Honig, B. H. (1986) The dielectric constant of a folded protein, *Biopolymers 25*, 2097−2119.
48. Simonson, T., and Brooks, C. L. (1996) Charge screening and the dielectric constant of proteins: insights from molecular dynamics, *J. Am. Chem. Soc. 118*, 8452−8458.
49. Im, W., Beglov, D., and Roux, B. (1998) Continuum solvation model: Electrostatic forces from numerical solutions to the Poisson−Bolztmann equation, *Comput. Phys. Commun. 111*, 59−75.
50. Roux, B. (1997) The influence of the membrane potential on the free energy of an intrinsic protein, *Biophys. J. 73*, 2980−2989.
51. Brooks, B. R., Bruccoleri, R. E., Olafson, B. D., States, D. J., Swaminathan, S., and Karplus, M. (1983) CHARMM: A program for macromolecular energy minimization and dynamics calculations, *J. Comput. Chem. 4*, 187−217.
52. Wada, A. (1976) The α-helix as an electric macro-dipole, *Adv. Biophys.*, 1−63.
53. Hol, W. G., van Duijnen, P. T., and Berendsen, H. J. (1978) The α-helix dipole and the properties of proteins, *Nature 273*, 443−446.
54. Hol, W. G. (1985) Effects of the α-helix dipole upon the functioning and structure of proteins and peptides, *Adv. Biophys.*, 133−165.
55. Lu, Z., and MacKinnon, R. (1994) Electrostatic tuning of Mg^{2+} affinity in an inward-rectifier K^+ channel, *Nature 371*, 243−246.
56. Wible, B. A., Taglialatela, M., Ficker, E., and Brown, A. M. (1994) Gating of inwardly rectifying K^+ channels localized to a single negatively charged residue, *Nature 371*, 246−249.
57. Lopatin, A. N., Makhina, E. N., and Nichols, C. G. (1995) The mechanism of inward rectification of potassium channels: "long-pore plugging" by cytoplasmic polyamines, *J. Gen. Physiol. 106*, 923−955.
58. Capener, C. E., Shrivastava, I. H., Ranatunga, K. M., Forrest, L. R., Smith, G. R., and Sansom, M. S. (2000) Homology modeling and molecular dynamics simulation studies of an inward rectifier potassium channel, *Biophys. J. 78*, 2929−2942.
59. Minor, D. L., Jr., Masseling, S. J., Jan, Y. N., and Jan, L. Y. (1999) Transmembrane structure of an inwardly rectifying potassium channel, *Cell 19*, 879−891.
60. Neyton, J., and Miller, C. (1988) Potassium blocks barium permeation through a calcium-activated potassium channel, *J. Gen. Physiol. 92*, 549−567.
61. Neyton, J., and Miller, C. (1988) Discrete Ba^{2+} block as a probe of ion occupancy and pore structure in the high-conductance Ca^{2+}-activated K^+ channel, *J. Gen. Physiol. 92*, 569−586.
62. Cuello, L. G., Romero, J. G., Cortes, D. M., and Perozo, E. (1998) pH-dependent gating in the *Streptomyces lividans* K^+ channel, *Biochemistry 37*, 3229−3236.
63. Perozo, E., Cortes, D. M., and Cuello, L. G. (1999) Structural rearrangements underlying K^+-channel activation gating, *Science 285*, 73−78.
64. Heginbotham, L., LeMasurier, M., Kolmakova-Partensky, L., and Miller, C. (1999) Single *Streptomyces lividans* K(+) channels. Functional asymmetries and sidedness of proton activation, *J. Gen. Physiol. 114*, 551−560.
65. Shrivastava, I. H., and Sanson, M. S. P. (2000) Simulation of ion permeation through a K channel: molecular dynamics of KcsA in a phospholipid bilayer, *Biophys. J. 78*, 557−570.
66. Bashford, D., and Karplus, M. (1990) pK_a's of ionizable groups in proteins: atomic detail from a continuum, electrostatic model, *Biochemistry 29*, 10219−10225.
67. Antosiewicz, J., McCammon, J. A., and Gilson, M. K. (1996) The determinants of pK_as in proteins, *Biochemistry 35*, 7819−7833.
68. Karshikoff, A., Spassov, A., Cowan, S. W., Ladenstein, R., and Schirmer, T. (1994) Electrostatic properties of two porin channels from *E. coli*, *J. Mol. Biol. 240*, 372−384.
69. Adcock, C., Smith, G. R., and Sansom, M. S. P. (1998) Electrostatics and the ion selectivity of ligand-gated channels, *Biophys. J. 75*, 1211−1222.
70. Borisenko, V., Sansom, M. S. P., and Woolley, G. A. (2000) Protonation of lysine residues inverts cation/anion selectivity in a model channel, *Biophys. J. 78*, 1335−1348.
71. Jiang, Y., and MacKinnon, R. (2000) The Barium Site in a Potassium Channel by X-ray Crystallography, *J. Gen. Physiol. 115*, 269−272.
72. Sigworth, F. J. (1993) Voltage gating of ion channels, *Q. Rev. Biophys. 27*, 1−40.
73. Chiu, S. W., Jakobsson, E., Subramaniam, S., and McCammon, J. A. (1991) Time-correlation analysis of simulated water motion in flexible and rigid gramicidin channels, *Biophys. J. 60*, 273−285.
74. Roux, B., and Karplus, M. (1991) Ion transport in a gramicidin-like channel: Dynamics and Mobility, *J. Phys. Chem. 95*, 4856−4868.
75. Sansom, M. S., Kerr, I. D., Breed, J., and Sankararamakrishnan, R. (1996) Water in channel-like cavities: structure and dynamics, *Biophys. J. 70*, 693−702.
76. Partenskii, M. B., and Jordan, P. C. (1992) Theoretical perspectives on ion-channel electrostatics: continuum and microscopic approaches, *Q. Rev. Biophys. 25*, 477−510.
77. Sansom, M. S. P., Smith, G. R., Adcock, C., and Biggin, P. C. (1997) The dielectric properties of water within model transbilayer pores, *Biophys. J. 73*, 2404−2415.
78. Roux, B. (1996) Valence Selectivity of the Gramicidin Channel: A Molecular Dynamics Free Energy Perturbation Study, *Biophys. J. 71*, 3177−3185.
79. Roux, B., Prod'hom, B., and Karplus, M. (1995) Ion transport in the gramicidin channel: Molecular dynamics study of single and double occupancy, *Biophys. J. 68*, 876−892.
80. Dorman, V., Partenskii, M. B., and Jordan, P. C. (1996) A semi-microscopic Monte Carlo study of permeation energetics in a gramicidin-like channel: The origin of cation selectivity, *Biophys. J. 70*, 121−134.
81. Dorman, V. L., Garofoli, S., and Jordan, P. C. (1999) Ionic interactions in multiply occupied channels, *Novartis Found. Symp.*, 153−169.
82. Andersen, O. S., and Koeppe, R. E. (1992) Molecular determinants of channel function, *Physiol. Rev. 72*, S89−S158.
83. Ketchem, R. R., Hu, W., and Cross, T. A. (1993) High-Resolution Conformation of Gramicidin A in Lipid Bilayer by Solid-State NMR, *Science 261*, 1457−1460.
84. Smith, R., Thomas, D. E., Atkins, A. R., Separovic, F., and Cornell, B. A. (1990) Solid-state ^{13}C-NMR studies of the effects of sodium ions on the gramicidin A ion channel, *Biochim. Biophys. Acta 1026*, 161−166.
85. Olah, G. A., Huang, H. W., and Liu, W. (1990) The thallium ion distribution in the gramicidin channel by X-ray diffraction, *Biophys. J. 57*, 99a.
86. Tian, F., Lee, K. C., Hu, W., and Cross, T. A. (1996) Monovalent cation transport: lack of structural deformation upon cation binding, *Biochemistry 35*, 11959−11966.
87. Woolf, T. B., and Roux, B. (1997) The Binding Site of Sodium in the Gramicidin A Channel: A Comparison of Molecular

Dynamics Simulations with Solid State NMR Data, *Biophys. J. 72*, 1930−1945.
88. Woolf, T. B., and Roux, B. (1996) Structure, Energetics and Dynamics of Lipid−Protein Interactions: A Molecular Dynamics Study of the Gramicidin A Channel in a DMPC Bilayer, *Proteins: Struct., Funct., Genet. 24*, 92−114.
89. Cooper, K. E., Jakobsson, E., and Wolynes, P. G. (1985) The theory of ion transport through membrane channels, *Prog. Biophys. Mol. Biol. 46*, 51−96.
90. Chung, S. H., Allen, T., Hoyles, M., and Kuyucak, S. (1999) Permeation of ions across the potassium channel: brownian dynamics studies, *Biophys. J. 77*, 2517−2533.
91. Schirmer, T., and Phale, P. (1999) Brownian dynamics simulation of ion flow through porin channels, *J. Mol. Biol. 294*, 1159−1168.
92. Im, W., Berneche, S., and Roux. B. (2000) A Grand Canonical Monte Carlo−Brownian Dynamics Algorithm for Simulating Ion Channels, *Biophys. J. 79*, 788−801.
93. Chen, D., Lear, J., and Eisenberg, R. (1997) Permeation through an open channel: Poisson−Nernst−Planck theory of a synthetic ionic channel, *Biophys. J. 72*, 97−116.
94. Kurnikova, M. G., Coalson, R. D., Graf, P., and Nitzan, A. (1999) A lattice relaxation algorithm for three-dimensional Poisson−Nernst−Planck theory with application to ion transport through the gramicidin A channel, *Biophys. J. 76*, 642−656.
95. MacKerell, A. D., Jr., Bashford, D., Bellot, M., Dunbrack, R. L., Evanseck, J. D., Field, M. J., Fischer, S., Gao, J., Guo, H., Joseph-McCarthy, D., Ha, S., Kuchnir, L., Kuczera, K., Lau, F. T. K., Mattos, C., Michnick, S., Ngo, T., Nguyen, D. T., Prodhom, B., Reiher, W. E., III, Roux, B., Schlenkrich, M., Smith, J., Stote, R., Straub, J., Watanabe, M., Wiorkiewicz-Kuczera, J., and Karplus, M. (1998) All-atom empirical potential for molecular modeling and dynamics studies of proteins, *J. Phys. Chems. B 102*, 3586−3616.
96. Deisenhofer, J., and Michel, H. (1989) The photosynthetic reaction center from the purple bacterium *Rhodopseudomonas viridis*, *Science 245*, 1463−1473.
97. Landolt-Marticorena, C., Williams, K. A., Deber, C. M., and Reithmeier, R. A. F. (1993) Non-random distribution of amino acids in the transmembrane segments of human type I single span membrane proteins, *J. Mol. Biol. 229*, 602−608.
98. Kumar, S., Bouzida, D., Swendsen, R. H., Kollman, P. A., and Rosenberg, J. M. (1992) The weighted histogram analysis method for free-energy calculations on biomolecules. I. The method, *J. Comput. Chem. 13*, 1011−1021.

BI001567V